

Eigenstate thermalization hypothesis and eigenstate-to-eigenstate fluctuations

Jae Dong Noh

Department of Physics, University of Seoul, Seoul 02504, Korea

(Dated: August 24, 2020)

We investigate the extent to which the eigenstate thermalization hypothesis (ETH) is valid or violated in the non-integrable and the integrable spin-1/2 XXZ chain. We perform the energy-resolved analysis of the statistical properties of matrix elements $\{O_{\gamma\alpha}\}$ of an observable \hat{O} in the energy eigenstate basis. The Hilbert space is coarse-grained into energy shells of width Δ_E , with which one can define a block submatrix $\hat{O}^{(b,a)}$ consisting of elements between eigenstates in the a th and b th shells. Each block submatrix is characterized by constant values of $E_{\gamma\alpha} = (E_\gamma + E_\alpha)/2 \simeq \bar{E}$ and $\omega_{\gamma\alpha} = (E_\gamma - E_\alpha) \simeq \omega$ up to Δ_E . We will show that all matrix elements within a block are statistically equivalent to each other in the non-integrable case. Their distribution is characterized by \bar{E} and ω , and follows the prediction of the ETH. In stark contrast, eigenstate-to-eigenstate fluctuations persist in the integrable case. Consequently, matrix elements $O_{\gamma\alpha}$ cannot be characterized by the energy parameters $E_{\gamma\alpha}$ and $\omega_{\gamma\alpha}$ only. Our result explains the origin for the breakdown of the fluctuation dissipation theorem in the integrable system. The eigenstate-to-eigenstate fluctuations sheds a new light on the meaning of the ETH.

I. INTRODUCTION

It is a fascinating question to ask whether an isolated quantum system can approach the thermal equilibrium state through the unitary time evolution since the birth of quantum mechanics [1, 2]. The thermalization requires that the Hamiltonian eigenstate expectation value of an observable should be equal to the equilibrium ensemble average and that temporal fluctuations and responses should be governed by the fluctuation dissipation theorem (FDT). It is accepted that the eigenstate thermalization hypothesis (ETH) provides a mechanism for the quantum thermalization [3–6].

An isolated quantum system is characterized by the Hamiltonian \hat{H} . Let $\{|\alpha\rangle\}$ and $\{E_\alpha\}$ be the energy eigenstates and the eigenvalues, respectively. The ETH [3, 7] assumes that matrix elements $O_{\gamma\alpha} \equiv \langle\gamma|\hat{O}|\alpha\rangle$ of an observable \hat{O} takes the form of

$$O_{\gamma\alpha} = O(E_{\gamma\alpha})\delta_{\gamma\alpha} + e^{-S(E_{\gamma\alpha})/2}f_O(E_{\gamma\alpha},\omega_{\gamma\alpha})R_{\gamma\alpha}, \quad (1)$$

where $E_{\gamma\alpha} \equiv (E_\gamma + E_\alpha)/2$, $\omega_{\gamma\alpha} \equiv E_\gamma - E_\alpha$, $S(E)$ is the thermodynamic entropy with the Boltzmann constant $k_B = 1$, $R_{\gamma\alpha}$'s are elements of a random matrix in the Gaussian orthogonal or unitary ensemble, and O and f_O are *smooth* functions characteristic of \hat{O} . It is worth stressing that the functions O and f_O should depend only on the energy parameters $E_{\gamma\alpha}$ and $\omega_{\gamma\alpha}$.

According to the ETH, a diagonal element, eigenstate expectation value, is written as

$$O_{\alpha\alpha} = O(E_\alpha) + e^{-S(E_\alpha)/2}f_O(E_\alpha,0)R_{\alpha\alpha}. \quad (2)$$

Since the entropy is an extensive quantity, the second term decays exponentially with the system size. Thus, the eigenstate expectation values are distributed around the microcanonical ensemble average with exponentially small fluctuations. The ETH for off-diagonal elements reads as

$$O_{\gamma\alpha(\neq\gamma)} = e^{-S(E_{\gamma\alpha})/2}f_O(E_{\gamma\alpha},\omega_{\gamma\alpha})R_{\gamma\alpha}. \quad (3)$$

They govern temporal fluctuations. The ETH form with $\gamma \neq \alpha$ guarantees that the FDT is valid at an energy eigenstate [5, 7–10].

The ETH ansatz has been tested extensively for the generic non-integrable and integrable systems [10–27]. The former is known to obey the ETH, while the latter does not obey the ETH [28]. We present a brief review on the numerical works testing the ETH.

For the diagonal elements, one may measure the difference $\delta O_\alpha = |O_{(\alpha+1)(\alpha+1)} - O_{\alpha\alpha}|$ in the eigenstate expectation values of neighboring eigenstates [16]. In the non-integrable systems, both their support and the mean value are found to decay exponentially with the system size [16, 20, 23, 25]. This behavior is consistent with Eq. (2). On the other hand, in the integral systems, the fluctuations have a nonvanishing support and their mean value decays at most algebraically with the system size [18, 25].

The off-diagonal elements are shown to follow the Gaussian distribution in the non-integrable systems. The variance is inversely proportional to the density of states and decays exponentially with the system size [25, 27]. These behaviors are also consistent with the ETH prediction. Using the variance and the density of states, one can estimate the functions $|f_O(E,\omega)|$ numerically [20].

The off-diagonal elements are also investigated in integrable systems. They do not follow the Gaussian distribution [17]. A model study [25] reported that they may follow a log-normal distribution. Interestingly, the variance is also found to be inversely proportional to the density of states as in the non-integrable systems. The product of the variance and the density of states seems to be a smooth function [25, 26, 29], which is reminiscent of the function $|f_O(E,\omega)|^2$ in the non-integrable systems.

The off-diagonal elements in the non-integrable and the integrable systems share two important features: (i) The variance is inversely proportional to the density of states, and (ii) it is a function of $E_{\gamma\alpha}$ and $\omega_{\gamma\alpha}$. These suggest that the off-diagonal elements in the integrable systems

may follow the ansatz of Eq. (3) with non-Gaussian random variables $R_{\gamma\alpha}$. We notice that the two common features are the essential ingredients leading to the FDT at the energy eigenstates [5, 9]. Apparently, it is contradictory to the known fact that the FDT is not valid in the integrable systems [30, 31].

In this paper, we perform the energy-resolved study of the statistical properties of matrix elements $\{O_{\gamma\alpha}\}$ of observables in the integrable and non-integrable spin-1/2 XXZ model. From the full matrix, one can construct a block submatrix \hat{O} whose column and row corresponds to the energy eigenstates belonging to energy shells of width Δ_E . Each block is characterized with constant energy parameters $E_{\gamma\alpha}$ and $\omega_{\gamma\alpha}$ up to Δ_E . Investigating the probability distribution of the elements within each block, one can test the ETH ansatz at various energy values. Furthermore, one can also investigate an eigenstate-to-eigenstate fluctuation from the statistics of matrix elements in each column separately. Our main result is that the eigenstate-to-eigenstate fluctuation vanishes in the non-integrable system and that it remains finite in the integrable system in the large system size limit.

The ETH ansatz in Eq. (3) for the off-diagonal elements requires that all matrix elements should be equivalent statistically within a block submatrix of almost constant $E_{\gamma\alpha}$ and $\omega_{\gamma\alpha}$. Otherwise, the function $f_O(E, \omega)$ cannot be a *smooth* function of the arguments. The non-vanishing eigenstate-to-eigenstate fluctuation disproves the existence of such a smooth function in the integrable system. Thus, it resolves the puzzle in regard to the FDT.

This paper is organized as follows. In Sec. II, we introduce the spin-1/2 XXZ Hamiltonian and the observables. We also explain the method to construct block submatrices. In Sec. III, we present the numerical results for the energy-resolved statistics for matrix elements within each submatrix. In Sec. IV, we investigate the eigenstate-to-eigenstate fluctuations in statistics of off-diagonal matrix elements. It will reveal the clear difference between the integrable and the non-integrable systems. We conclude the paper with summary and discussions in Sec. V.

II. MODEL SYSTEM AND NUMERICAL SETUP

We study the XXZ spin model in a one-dimensional lattice of L sites under the periodic boundary condition. Let $\hat{\sigma}_l^p$ be the Pauli matrix in the direction p ($= x, y, z$) at site l ($= 1, \dots, L$). With $\hat{h}_{l,m} \equiv -\frac{J}{2}(\hat{\sigma}_l^x \hat{\sigma}_m^x + \hat{\sigma}_l^y \hat{\sigma}_m^y + \Delta \hat{\sigma}_l^z \hat{\sigma}_m^z)$, the XXZ Hamiltonian is given by

$$\hat{H} = \frac{1}{1+\lambda} \sum_{l=1}^L [\hat{h}_{l,l+1} + \lambda \hat{h}_{l,l+2}], \quad (4)$$

where Δ is an anisotropy parameter and λ denotes the relative strength of the next nearest neighbor interactions. The overall coupling constant J will be set to

unity so that the energy becomes dimensionless. The integrability is controlled by λ . The Hamiltonian is integrable when $\lambda = 0$, and non-integrable with nonzero λ [9, 21, 24].

The Hamiltonian commutes with the total magnetization operator in the z direction, the translation operator, the spatial reflection operator, and the spin inversion operator. Especially, in the translationally invariant subspace with zero magnetization, all the symmetry operators mutually commute [32]. We focus our attention on the translationally invariant subspace with zero magnetization that are even under the spatial reflection and the spin inversion, which will be called the maximum symmetry sector (MSS) [32]. The Hilbert space dimensions of the MSS are $D = 2518, 8359, \text{ and } 28968$ for $L = 20, 22, \text{ and } 24$, respectively. In this paper, we present the numerical results obtained with $\lambda = 0$ (integrable case) and $\lambda = 1$ (non-integrable case) with fixed $\Delta = 1/2$.

We numerically diagonalize the Hamiltonian in the MSS to obtain the energy eigenvalues $\{E_\alpha\}$ and the eigenstates $\{|\alpha\rangle\}$ with $\alpha = 1, \dots, D$ [32, 33]. The eigenstates are arranged in the ascending order of the energy eigenvalues. Using the eigenvalue spectrum, we define a function

$$\bar{E}(\beta) = \frac{\sum_{\gamma} E_{\gamma} e^{-\beta E_{\gamma}}}{\sum_{\gamma} e^{-\beta E_{\gamma}}}. \quad (5)$$

If the system is thermal, $\bar{E}(\beta)$ corresponds to the equilibrium canonical ensemble average of the energy at the inverse temperature β . One can assign the temperature to each energy eigenstate using the relation $\bar{E}(\beta) = E_{\alpha}$. Even in the nonthermal case, the function is useful since one can parameterize the energy eigenvalue with an intensive variable β using the relation $\bar{E}(\beta) = E_{\alpha}$. We will call the parameter β the inverse temperature in both cases for convenience.

Once all eigenvectors are obtained, it is straightforward to calculate the matrix elements $O_{\gamma\alpha}$ of an observable \hat{O} [32]. For a detailed study, we introduce a block submatrix. To a given value of β and $\bar{E} = \bar{E}(\beta)$, we define an energy shell \mathcal{S}_a as the subspace consisting of energy eigenstates whose eigenvalues are within the interval $[\bar{E} + (a - \frac{1}{2})\Delta_E : \bar{E} + (a + \frac{1}{2})\Delta_E]$ with $a = 0, \pm 1, \pm 2, \dots$. The energy resolution Δ_E is taken to be a constant independent of the system sizes. The number of energy eigenstates within a shell \mathcal{S}_a is denoted by \mathcal{N}_a . A block submatrix $\hat{O}^{(b,a)}(\beta)$ is defined as a $(\mathcal{N}_b \times \mathcal{N}_a)$ matrix consisting of elements $O_{\gamma\alpha}$ with $|\gamma\rangle \in \mathcal{S}_b$ and $|\alpha\rangle \in \mathcal{S}_a$. All elements of $\hat{O}^{(b,a)}$ are characterized by constant $E_{\gamma\alpha} \simeq \bar{E}(\beta) + (a + b)\Delta_E/2$ and $\omega_{\gamma\alpha} \simeq (b - a)\Delta_E$ up to Δ_E . We illustrate the block submatrix structure in Fig. 1.

As an observable, we choose the nearest neighbor interaction energy

$$\hat{O}_1 = \frac{1}{\sqrt{L}} \sum_l \hat{\sigma}_l^z \hat{\sigma}_{l+1}^z \quad (6)$$

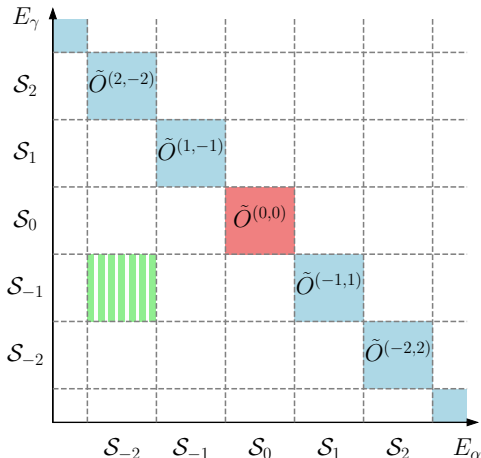


FIG. 1. Illustration of the block submatrix structure. Each square corresponds to a block submatrix. The shaded blocks are studied in Sec. III. The stripes represent columns in a block submatrix which will be studied in Sec. IV.

and the zero momentum distribution function

$$\hat{O}_2 = \frac{1}{L} \sum_{l,m} \hat{\sigma}_l^+ \hat{\sigma}_m^- \quad (7)$$

Notice that the nearest neighbor interaction energy is normalized with \sqrt{L} instead of L . With this choice, the Hilbert-Schmidt norm becomes L -independent so that the ETH analysis becomes convenient [25, 34].

III. NUMERICAL RESULTS

A. Diagonal blocks

We study the matrix elements in a diagonal block $\tilde{O}^{(0,0)}(\beta)$ which is characterized with $E_{\gamma\alpha} \simeq \bar{E}(\beta)$ and $\omega_{\gamma\alpha} \simeq 0$. A diagonal block includes both diagonal and off-diagonal matrix elements. Thus, one can compare the distributions of both quantities. Figure 2 presents the histograms of the diagonal and off-diagonal elements at $\beta = 0.0$ for \hat{O}_1 and 0.2 for \hat{O}_2 .

Before proceeding, we remark on the effect of the energy shell size Δ_E (see also discussions in Ref. [27]). In Fig. 2, we compare the histograms obtained with $\Delta_E = 0.1, 0.3, 0.5,$ and 1.0 . There is a tradeoff between small and large Δ_E . For small Δ_E , one can study the intrinsic statistical property at a given energy scale. However, statistics becomes worse because an energy shell includes a fewer eigenstates. As Δ_E increases, one can expect better statistics but a systematic correction arises. For instance, in Fig. 2 (a) and (e) a plateau appears at the center of the histogram for the diagonal elements,

which broadens as Δ_E increases. A diagonal element $\langle \alpha | \hat{O} | \alpha \rangle$ is an energy eigenstate expectation value. With finite Δ_E , the histogram is given by the superposition of the intrinsic distribution functions at different energy values. The plateau reflects the extrinsic fluctuations due to the energy dispersion. In this section, we will use the intermediate value of $\Delta_E = 0.3$ at which the extrinsic fluctuations are weak.

The diagonal and off-diagonal elements follows the Gaussian distribution for both observables in the non-integrable case. In Figs. 2(b) and (f), we compare the distribution function of the off-diagonal elements and the symmetric Gaussian distribution function of the same variance. The ETH predicts that the variance of the diagonal elements are twice that of the off-diagonal elements [20, 23]. We compare in Figs. 2(a) and (e) the distribution of the diagonal elements and the Gaussian distribution function with variance doubled. The center of the Gaussian is shifted to the mean value of the diagonal elements. The perfect agreement confirms the ETH ansatz in Eq. (1) for $\omega_{\gamma\alpha} \simeq 0$.

In the integrable case, the distribution deviates from the ETH ansatz. The distribution functions of diagonal elements, shown in Figs. 2(c) and (g), are asymmetric. The distribution functions of off-diagonal elements, shown in Figs. 2(d) and (h), are symmetric but different from the Gaussian distribution. It was reported in Ref. [25] that \hat{O}_1 may follow a log-normal distribution. However, our data are fitted better with a stretched exponential distribution in the tail part. We suspect that the distribution may be not universal in the integrable system.

The variance of off-diagonal elements, denoted by $\sigma_o^2[\hat{O}]$ with o standing for off-diagonal elements, depends on the system size L . We investigate the size dependence at $\beta = 0.0, 0.1, 0.2,$ and 0.3 . The ETH predicts that

$$\sigma_o^2[\hat{O}] = e^{-S(\bar{E})} |f_O(\bar{E}, \omega = 0)|^2. \quad (8)$$

The system size dependence comes into play through the entropy function $S(\bar{E}(\beta))$. It can be estimated as $S(\bar{E}) = \ln \mathcal{D}(\bar{E})$ where $\mathcal{D}(\bar{E}) = \mathcal{N}_0/\Delta_E$ is the density of the states at the energy shell \mathcal{S}_0 .

The variance multiplied by \mathcal{D} is plotted in Fig. 3 as a function of β . In the non-integrable case, the curves from different system sizes $L = 20, 22,$ and 24 tend to align along a single curve for both operators \hat{O}_1 and \hat{O}_2 . They represent the functions $|f_O(\bar{E}(\beta), \omega = 0)|^2$ of the operators \hat{O}_1 and \hat{O}_2 . This behavior is fully consistent with Eq. (8). Most of previous works investigated the scaling of the off-diagonal elements around the infinite temperature state ($\beta = 0$) where \mathcal{D} is proportional to the dimensionality of the total Hilbert space [20, 23, 25]. Our work confirms the the scaling form of Eq. (8) at finite temperature states.

In the integrable system, the scaled variances from different system sizes are rather scattered. Nevertheless, from the plot in Fig. 3(b) for $L = 22$ and 24 we expect that the off-diagonal elements of \hat{O}_1 follow the same

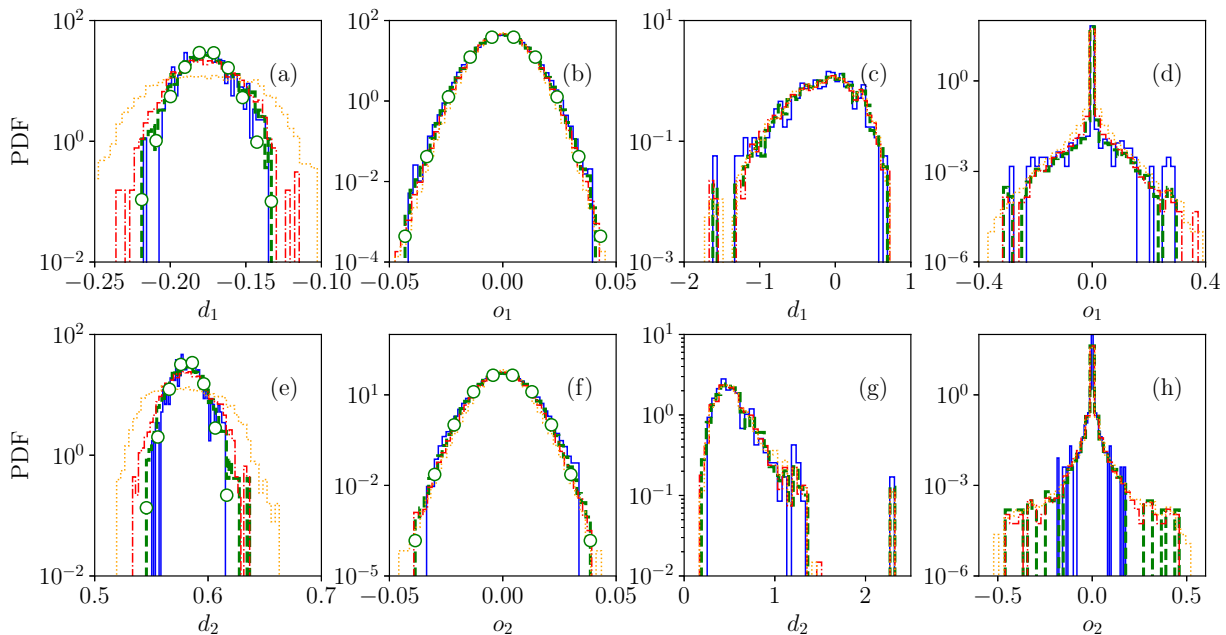


FIG. 2. Histograms of the matrix elements of \hat{O}_1 (upper row) and \hat{O}_2 (lower row) in the diagonal blocks $\tilde{O}^{(0,0)}(\beta)$ at $\beta = 0.0$ for \hat{O}_1 and 0.2 for \hat{O}_2 . Panels (a), (b), (e), and (f) are for the non-integrable case with $\lambda = 1$, and the others for the integrable case with $\lambda = 0$. The energy shell widths are $\Delta_E = 0.1$ (blue solid), 0.3 (green dashed), 0.5 (red dashed-dotted), and 1.0 (orange dotted). Diagonal and off-diagonal matrix elements of \hat{O}_i are denoted as d_i and o_i , respectively.

scaling form of Eq. (8) when the systems sizes are large enough. The data for \hat{O}_2 are more scattered. However, further analysis in the following subsection support that the scaling form $\sigma_o^2 \propto 1/D$ is also valid for \hat{O}_2 .

We remark that the scaling form in Eq. (8) alone is not the evidence for the ETH. We have already shown that the distribution function of the off-diagonal elements in the integrable system is far from the Gaussian. What is shown in Fig. 3 is that the fluctuation amplitude of the off-diagonal elements scales as $1/D$ in both integrable and non-integrable systems.

B. Off-diagonal blocks

We investigate matrix elements of off-diagonal blocks $\tilde{O}^{(b,a)}(\beta)$ with $b \neq a$. As explained in Sec. II, a block submatrix $\tilde{O}^{(b,a)}(\beta)$ consists of matrix elements $\{O_{\gamma\alpha}\}$ with $E_\alpha \simeq \bar{E}(\beta) + a\Delta_E$ and $E_\gamma \simeq \bar{E}(\beta) + b\Delta_E$. Off-diagonal blocks with $b \neq a$ include only off-diagonal matrix elements. Specifically, we will consider the block submatrices with $b = -a = 1, 2, \dots$ in which $E_{\gamma\alpha} \simeq \bar{E}(\beta)$ and $\omega_{\gamma\alpha} \simeq \omega = 2b\Delta_E$. They are represented by the shaded blocks in Fig. 1. We have measured the probability distribution and the variance at each off-diagonal block. The numerical results at $\beta = 0$ and 0.2 are presented in Fig. 4 for the non-integrable case and Fig. 5 for the integrable case.

Non-integrable case.— At all values of $\bar{E}(\beta)$ and ω , matrix elements follow the symmetric Gaussian distri-

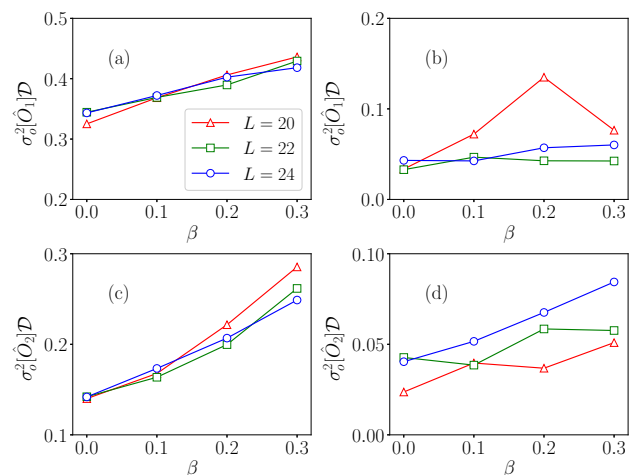


FIG. 3. Scaled variance of off-diagonal elements within a diagonal block $\tilde{O}^{(0,0)}(\beta)$. The variance is multiplied by the density of states $\mathcal{D}(\bar{E}(\beta))$. Panels (a) and (c) correspond to the non-integrable case ($\lambda = 1$), while the others corresponds to the integrable case ($\lambda = 0$). The system sizes are $L = 20$, 22, and 24.

bution. In Fig. 4(a) and (c), we compare the numerical distribution function with the symmetric Gaussian of the same variance. The agreement is almost perfect, which indicates the validity of the ETH.

The variances of the elements within $\tilde{O}^{(b,-b)}(\beta)$ at dif-

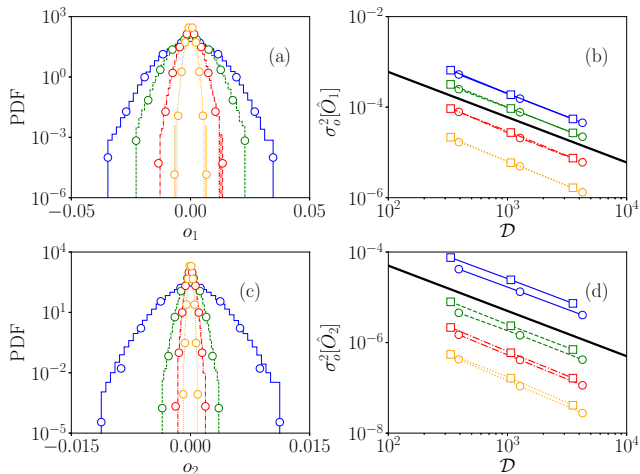


FIG. 4. Numerical data for the off-diagonal blocks $\tilde{O}^{(b,-b)}(\beta)$ with $\omega = 2b\Delta_E$ with $b = 4$ (blue solid), 8 (green dashed), 12 (red dashed dotted), and 16 (orange dotted) in the *non-integrable* case. (a) and (c) show the probability distribution functions at $\beta = 0$ for \hat{O}_1 and \hat{O}_2 , respectively. The probability distribution is compared with the Gaussian of the same variance marked with symbols. We plot the variances against the density of states $\mathcal{D}(\bar{E}(\beta))$ in (b) for \hat{O}_1 and (d) for \hat{O}_2 . Circular (square) symbols represent the data at $\beta = 0$ (0.2). The thick line of slope -1 is a guide to the eye.

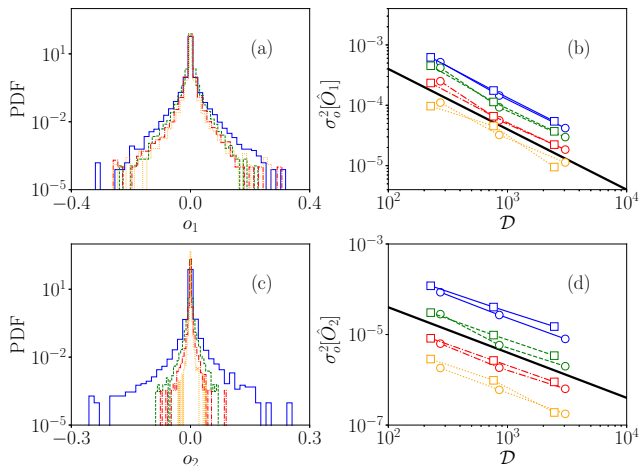


FIG. 5. The same plot as in Fig. 4 for the *integrable* case.

ferent system sizes $L = 20, 22,$ and 24 are plotted as a function of the density of states $\mathcal{D}(\bar{E}(\beta))$ in Figs. 4(b) and (d). For both observables \hat{O}_1 and \hat{O}_2 , the variances are inversely proportional to the density of states at all values of $\beta = 0$ and 0.2 , and ω . Their slopes correspond to the functions $|f_O(\bar{E}, \omega)|^2$. These numerical results, together with those in the preceding subsections, strongly supports for ETH ansatz in Eq. (1) at all energy scales.

Integrable case. – We have performed the same analysis in the integrable system. The histograms for \hat{O}_1 and \hat{O}_2 are presented in Fig. 5(a) and (c), respectively. As in the

case with $\omega = 0$ (Figs. 2(d) and (h)), the distribution is non-Gaussian. The distribution functions in the tail decay slower than an exponential function.

We also investigate the finite-size scaling behavior of the variance. We have measured the variance of the matrix elements in each off-diagonal block $\tilde{O}^{(b,-b)}(\beta)$ at different system sizes $L = 20, 22,$ and 24 . They are plotted against the density of states $\mathcal{D}(\bar{E}(\beta))$ in Figs. 5(b) and (d). The overall behavior is consistent with the scaling $\sigma_o^2(\hat{O}) \propto 1/\mathcal{D}$ for both observables. Such a scaling was also reported for the integrable systems at the center of the energy spectrum [17, 25]. In comparison to Fig. 4, the data suffer from small fluctuations from the scaling behavior. They are consistent with the results shown in Figs. 3(b) and (d).

Summarizing the results in this subsection, we have investigated the statistical property of off-diagonal matrix elements $\{O_{\gamma\alpha}\}$ within each block characterized with $E_{\gamma\alpha} \simeq \bar{E}(\beta)$ and $\omega_{\gamma\alpha} \simeq \omega$. We have confirmed that the non-integrable system follows the prediction of the ETH in Eq. (3) with Gaussian random variables $R_{\gamma\alpha}$. In the integrable systems, the distribution function is non-Gaussian. However, the variance is shown to be inversely proportional to the density of states with a slope depending on \bar{E} and ω .

IV. EIGENSTATE-TO-EIGENSTATE FLUCTUATIONS

The ETH ansatz in Eq. (1) is a strong requirement that all matrix elements involving nearby energy eigenstates should be statistically equivalent with vanishing eigenstate-to-eigenstate fluctuations. The equivalence for the diagonal elements has been tested by performing the finite size scaling analysis of $\delta O_\alpha = |O_{(\alpha+1)(\alpha+1)} - O_{\alpha\alpha}|$ [16, 19, 23] and of the deviation of eigenstate expectation values from the microcanonical ensemble average [21]. However, off-diagonal elements have been studied only in the *coarse-grained level*. The eigenstate-to-eigenstate fluctuations for off-diagonal elements have not been studied both for the non-integrable and the integrable systems, which will be addressed in this section.

We consider a block submatrix $\tilde{O}^{(b,-b)}(\beta)$ characterized with $E_{\gamma\alpha} \simeq \bar{E}(\beta)$ and $\omega_{\gamma\alpha} \simeq \omega = 2b\Delta_E$. Each column, represented as a stripe in Fig. 1, corresponding to an energy eigenstate $|\alpha\rangle \in \mathcal{S}_{-b}$ is a set of off-diagonal matrix elements $\{O_{\gamma\alpha}\}$ where $|\gamma\rangle \in \mathcal{S}_b$. Instead of the moment of all elements in a block, we measure the second moment M_2 column by column. Then, we can access the eigenstate-to-eigenstate fluctuations from the distribution of the columnar second moments.

In Fig. 6, we present the histogram of the normalized columnar second moments $m \equiv M_2/\langle M_2 \rangle$ where $\langle M_2 \rangle$ is the mean value of the second moments of all columns within a block submatrix. In the non-integrable case with $\lambda = 1$, shown in Figs. 6(a) and (c), the distribution functions are peaked around $m \simeq 1.0$. Furthermore, the

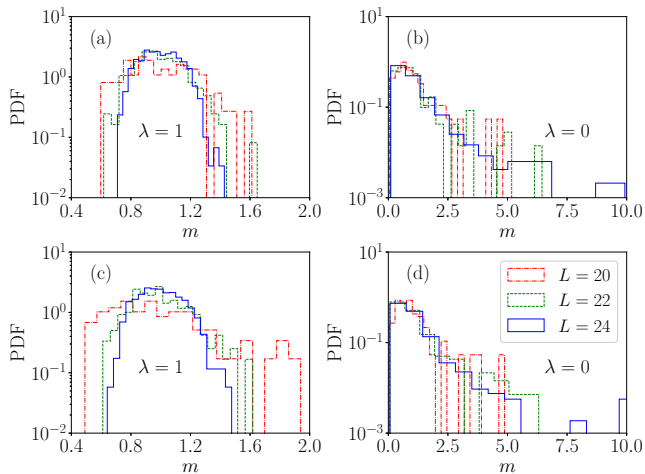


FIG. 6. Histogram of the normalized columnar second moments, $m = M_2/\langle M_2 \rangle$, of off-diagonal elements within a block $\tilde{O}^{(b,-b)}(\beta)$ with $\beta = 0.0$ and $b = 8$. Panels (a) and (b) are for the observable \hat{O}_1 , and (c) and (d) are for \hat{O}_2 . Panels (a) and (c) are for the non-integrable case and (b) and (d) are for the integrable case. At $L = 24$, the sizes of the block submatrix are (921×829) in the non-integrable case and (712×776) in the integrable case.

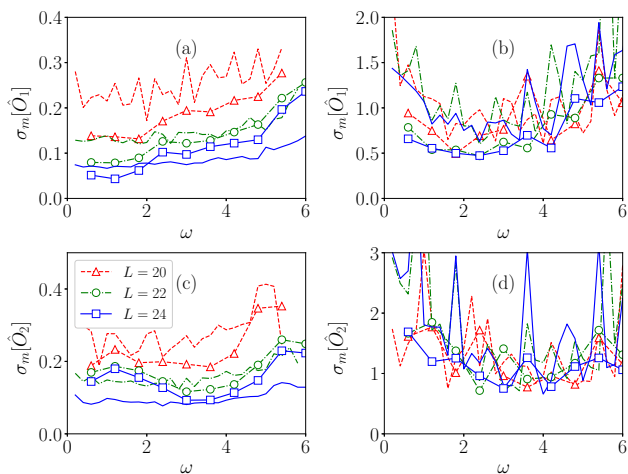


FIG. 7. Standard deviation $\sigma_m[\hat{O}_i]$ of the normalized columnar second moments of off-diagonal elements in $\tilde{O}_{b,-b}(\beta)$ with $\beta = 0$. The data are plotted as a function of $\omega = 2b\Delta_E$. Lines with symbols represent the data with $\Delta_E = 0.3$, while lines without symbols represent the data with $\Delta_E = 0.1$. The panels (a) and (c) are for the non-integrable system, and (b) and (d) are for the integrable system.

peaks become narrower as the system size L increases.

The integrable system ($\lambda = 0$) exhibits strikingly distinct behaviors. The distribution functions shown in Figs. 6(b) and (d) have a heavy tail. Furthermore, we cannot find any signature suggesting that the width of the distribution may decrease with the system sizes.

We quantify the eigenstate-to-eigenstate fluctuation

with the standard deviation of m . The numerical data are plotted in Fig. 7. In the non-integrable case ($\lambda = 1$), the standard deviation decreases as the system size increases at all values of $\omega = 2b\Delta_E$. On the other hand, in the integrable case ($\lambda = 1$), the standard deviation tends to converge to nonzero values.

We remark that there are two sources of the fluctuations leading to nonzero values of σ_m . First of all, the intrinsic eigenstate-to-eigenstate fluctuations are responsible for them, which are the subject of the current study. In addition, since Δ_E is finite, the extrinsic fluctuations due to the energy dispersion among eigenstates also contribute to the fluctuations.

In order to reduce the effect from the extrinsic fluctuations, we have also measured the standard deviation of m using the smaller values of the energy shell width $\Delta_E = 0.1$. The two data sets from $\Delta_E = 0.1$ and 0.3 are compared in Fig. 7, which gives a hint on the nature of the intrinsic fluctuations. In the non-integrable case, the relative standard deviation decays more rapidly with the system size at $\Delta_E = 0.1$. In the integrable case, the relative fluctuation becomes even stronger at $\Delta_E = 0.1$.

Based on the numerical results, we conclude that the intrinsic eigenstate-to-eigenstate fluctuations vanish in the non-integrable system while they persist in the integrable system in the infinite size limit. Our result provides a strong support for the ETH ansatz for off-diagonal elements in the non-integrable systems. It also reveals that the off-diagonal elements in the integrable system do not obey the ETH not only because of the non-Gaussian nature but also because of the eigenstate-to-eigenstate fluctuations.

V. SUMMARY AND DISCUSSIONS

In summary, we have performed a thorough numerical analysis on the statistical property of matrix elements $\{O_{\gamma\alpha}\}$ of observables in the energy eigenstate basis of the integrable and non-integrable spin-1/2 XXZ chain. Introducing the coarse-graining scheme with the block submatrix, we have characterized the statistical property in the energy-resolved way. Our study confirms that the ETH ansatz characterizes the statistics in the non-integrable model at all energy scales. In various regions with different values of $E_{\gamma\alpha} \simeq \bar{E}$ and $\omega_{\gamma\alpha} \simeq \omega$, the moments and the distribution functions are shown to follow the prediction of the ETH.

Statistics in the integrable system is subtle. Both the diagonal and off-diagonal elements do not follow the distributions predicted by the ETH. On the other hand, the variance of off-diagonal elements within blocks seems to be well-defined and inversely proportional to the density of states at $E = \bar{E}(\beta)$. However, we discover that the eigenstate-to-eigenstate fluctuations are relevant in the integrable system. Figures 6 and 7 show that the eigenstate-to-eigenstate fluctuations are of the same order of magnitude as the overall fluctuations. It disproves

a scaling form such as in Eq. (8).

In the non-integrable system, the eigenstate-to-eigenstate fluctuations vanishes in the large system size limit. It implies that all the matrix elements $O_{\gamma\alpha}$'s with $E_{\gamma\alpha} \simeq \bar{E}$ and $\omega_{\gamma\alpha} \simeq \omega$ are statistically equivalent to each others. It provides a strong justification of the ETH ansatz shown in Eq. (3).

The eigenstate-to-eigenstate fluctuation is important to understand the origin for the breakdown of the FDT in the integrable system. When a system is prepared initially at an energy eigenstate $|\alpha\rangle$, a dynamic correlation function $\bar{S}(\omega) = \int_{-\infty}^{\infty} dt \langle \hat{O}(t) \hat{O}(0) \rangle e^{i\omega t}$ of an observable \hat{O} in the frequency domain is given by [35]

$$\bar{S}(\omega) = 2\pi \sum_{\gamma \neq \alpha} O_{\alpha\gamma} O_{\gamma\alpha} \delta(\omega - \omega_{\gamma\alpha}). \quad (9)$$

In the thermal equilibrium systems in the Gibbs state, the correlation function and the response function are related through the FDT [36]. Recently, it is shown that the FDT is also valid in an energy eigenstate when a system obeys the ETH [5, 9, 10]. The derivation relies on the properties that the second moment of $O_{\gamma\alpha}$'s is a smooth function of $E_{\gamma\alpha}$ and $\omega_{\gamma\alpha}$ and is inversely proportional to the density of states $\mathcal{D}(E_{\gamma\alpha})$. We notice that the numerical results of Sec. IIIB and the literatures, e.g., Ref. [25], in the coarse-grained energy scale show that the integrable systems have the same properties. It is puzzling because the integrable system is known to violate the FDT [30, 31]. This puzzle is resolved by the

eigenstate-to-eigenstate fluctuations.

The FDT can be casted in the form of the Kubo-Martin-Schwinger (KMS) relation [36, 37]

$$\bar{S}(\omega) = e^{\beta\omega} \bar{S}(-\omega). \quad (10)$$

It constrains that $\frac{1}{\omega} \ln[\bar{S}(\omega)/\bar{S}(-\omega)]$ should be independent of ω and equal to the inverse temperature β . The correlation function $\bar{S}(\omega)$ in Eq. (9) involves a columnar second moment. In the presence of the eigenstate-to-eigenstate fluctuations, the columnar second moment has an explicit eigenstate dependence, which results in a ω dependence in $\frac{1}{\omega} \ln[\bar{S}(\omega)/\bar{S}(-\omega)]$ in general. It explains the reason why the FDT is not valid in the integrable systems.

The eigenstate-to-eigenstate fluctuations presented in Fig. 7 depend on the choice of Δ_E . In order to reduce the effect of the extrinsic fluctuations and achieve a good statistics, one need to choose a smaller value of Δ_E at larger system sizes. We leave a more quantitative study on the finite size scaling property at larger system sizes as a future work.

ACKNOWLEDGMENTS

This work is supported by the National Research Foundation of Korea (KRF) grant funded by the Korea government (MSIP) [Grant No. 2019R1A2C1009628].

-
- [1] J. von Neumann, Beweis des Ergodensatzes und des H-Theorems in der neuen Mechanik, *Z. Phys.* **57**, 30 (1929).
- [2] J. von Neumann, Proof of the ergodic theorem and the H-theorem in quantum mechanics, *Eur. Phys. J. H* **35**, 201 (2010).
- [3] M. Srednicki, Thermal fluctuations in quantized chaotic systems, *J. Phys. A* **29**, L75 (1996).
- [4] M. Rigol, V. Dunjko, and M. Olshanii, Thermalization and its mechanism for generic isolated quantum systems, *Nature* **452**, 854 (2008).
- [5] L. D'Alessio, Y. Kafri, A. Polkovnikov, and M. Rigol, From quantum chaos and eigenstate thermalization to statistical mechanics and thermodynamics, *Adv. Phys.* **65**, 239 (2016).
- [6] J. M. Deutsch, Eigenstate thermalization hypothesis, *Rep. Prog. Phys.* **81**, 082001 (2018).
- [7] M. Srednicki, The approach to thermal equilibrium in quantized chaotic systems, *J. Phys. A* **32**, 1163 (1999).
- [8] E. Khatami, G. Pupillo, M. Srednicki, and M. Rigol, Fluctuation-Dissipation Theorem in an Isolated System of Quantum Dipolar Bosons after a Quench, *Phys. Rev. Lett.* **111**, 050403 (2013).
- [9] J. D. Noh, T. Sagawa, and J. Yeo, Numerical Verification of the Fluctuation-Dissipation Theorem for Isolated Quantum Systems, *Phys. Rev. Lett.* **125**, 050603 (2020).
- [10] A. Schuckert and M. Knap, Probing eigenstate thermalization with the emergence of fluctuation-dissipation relations in quantum simulators, arXiv:2007.10347 (2020).
- [11] M. Rigol, Breakdown of Thermalization in Finite One-Dimensional Systems, *Phys. Rev. Lett.* **103**, 100403 (2009).
- [12] R. Steinigeweg, J. Herbrych, and P. Prelovšek, Eigenstate thermalization within isolated spin-chain systems, *Phys. Rev. E* **87**, 012118 (2013).
- [13] T. N. Ikeda, Y. Watanabe, and M. Ueda, Finite-size scaling analysis of the eigenstate thermalization hypothesis in a one-dimensional interacting Bose gas, *Phys. Rev. E* **87**, 012125 (2013).
- [14] R. Steinigeweg, A. Khodja, H. Niemeyer, C. Gogolin, and J. Gemmer, Pushing the Limits of the Eigenstate Thermalization Hypothesis towards Mesoscopic Quantum Systems, *Phys. Rev. Lett.* **112**, 130403 (2014).
- [15] W. Beugeling, R. Moessner, and M. Haque, Finite-size scaling of eigenstate thermalization, *Phys. Rev. E* **89**, 042112 (2014).
- [16] H. Kim, T. N. Ikeda, and D. A. Huse, Testing whether all eigenstates obey the eigenstate thermalization hypothesis, *Phys. Rev. E* **90**, 052105 (2014).
- [17] W. Beugeling, R. Moessner, and M. Haque, Off-diagonal matrix elements of local operators in many-body quantum systems, *Phys. Rev. E* **91**, 012144 (2015).
- [18] V. Alba, Eigenstate thermalization hypothesis and in-

- tegrability in quantum spin chains, *Phys. Rev. B* **91**, 155123 (2015).
- [19] R. Mondaini, K. R. Fratus, M. Srednicki, and M. Rigol, Eigenstate thermalization in the two-dimensional transverse field Ising model, *Phys. Rev. E* **93**, 032104 (2016).
- [20] R. Mondaini and M. Rigol, Eigenstate thermalization in the two-dimensional transverse field Ising model. II. Off-diagonal matrix elements of observables, *Phys. Rev. E* **96**, 012157 (2017).
- [21] T. Yoshizawa, E. Iyoda, and T. Sagawa, Numerical Large Deviation Analysis of the Eigenstate Thermalization Hypothesis, *Phys. Rev. Lett.* **120**, 200604 (2018).
- [22] C. Nation and D. Porras, Off-diagonal observable elements from random matrix theory: distributions, fluctuations, and eigenstate thermalization, *New J. Phys.* **20**, 103003 (2018).
- [23] D. Jansen, J. Stolpp, L. Vidmar, and F. Heidrich-Meisner, Eigenstate thermalization and quantum chaos in the Holstein polaron model, *Phys. Rev. B* **99**, 155130 (2019).
- [24] J. D. Noh, E. Iyoda, and T. Sagawa, Heating and cooling of quantum gas by eigenstate Joule expansion, *Phys. Rev. E* **100**, 010106(R) (2019).
- [25] T. LeBlond, K. Mallayya, L. Vidmar, and M. Rigol, Entanglement and matrix elements of observables in interacting integrable systems, *Phys. Rev. E* **100**, 062134 (2019).
- [26] M. Brenes, T. LeBlond, J. Goold, and M. Rigol, Eigenstate Thermalization in a Locally Perturbed Integrable System, [arXiv:2004.04755](https://arxiv.org/abs/2004.04755) (2020).
- [27] J. Richter, A. Dymarsky, R. Steinigeweg, and J. Gemmer, The eigenstate thermalization hypothesis beyond standard indicators: emergence of random-matrix behavior at small frequencies, [arXiv:2007.15070](https://arxiv.org/abs/2007.15070) (2020).
- [28] There are systems which exhibit many body localizations or scars, which do not follow the classification scheme in terms of the integrability. They are not discussed in this work.
- [29] K. Mallayya and M. Rigol, Heating Rates in Periodically Driven Strongly Interacting Quantum Many-Body Systems, *Phys. Rev. Lett.* **123**, 240603 (2019).
- [30] L. Foini, L. F. Cugliandolo, and A. Gambassi, Fluctuation-dissipation relations and critical quenches in the transverse field Ising chain, *Phys. Rev. B* **84**, 212404 (2011).
- [31] L. Foini, L. F. Cugliandolo, and A. Gambassi, Dynamic correlations, fluctuation-dissipation relations, and effective temperatures after a quantum quench of the transverse field Ising chain, *J. Stat. Mech.* , P09011 (2012).
- [32] J.-H. Jung and J. D. Noh, Guide to Exact Diagonalization Study of Quantum Thermalization, *J. Korean Phys. Soc.* **76**, 670 (2020).
- [33] A. W. Sandvik, Computational Studies of Quantum Spin Systems, *AIP Conf. Proc.* **1297**, 135 (2010).
- [34] M. Mierzejewski and L. Vidmar, Quantitative Impact of Integrals of Motion on the Eigenstate Thermalization Hypothesis, *Phys. Rev. Lett.* **124**, 040603 (2020).
- [35] In general, the FDT is formulated for two different operators. In this work, it suffices to consider the autocorrelation function.
- [36] G. F. Mazenko, *Nonequilibrium Statistical Mechanics* (Wiley-VCH, Weinheim, 2006).
- [37] R. Haag, N. M. Hugenholtz, and M. Winnink, On the Equilibrium states in quantum statistical mechanics, *Commun. Math. Phys.* **5**, 215 (1967).